applied sciences

MDPI

Article

# Amorphous Oxide Thin Film Transistors with Nitrogen-Doped Hetero-Structure Channel Layers

**Haiting Xie, Guochao Liu, Lei Zhang, Yan Zhou and Chengyuan Dong ***

Department of Electronic Engineering, Shanghai Jiao Tong University, Shanghai 200240, China; haitingx@126.com (H.X.); lgc_0801@sjtu.edu.cn (G.L.); zlsj15@sjtu.edu.cn (L.Z.); zhou_yan@sjtu.edu.cn (Y.Z.)

* Correspondence: cydong@sjtu.edu.cn; Tel.: +86-21-34207894

Received: 7 September 2017; Accepted: 17 October 2017; Published: 24 October 2017

**Abstract:** The nitrogen-doped amorphous oxide semiconductor (AOS) thinfilm transistors (TFTs) with double-stacked channel layers (DSCL) were prepared and characterized. The DSCL structure was composed of nitrogen-doped amorphous InGaZnO and InZnO films (a-IGZO:N/a-IZO:N or a-IZO:N/a-IGZO:N) and gave the corresponding TFT devices large field-effect mobility due to the presence of double conduction channels. The a-IZO:N/a-IGZO:N TFTs, in particular, showed even better electrical performance ($\mu_{FE}$ = 15.0 $cm^2 \cdot V^{-1} \cdot s^{-1}$, SS = 0.5 V/dec, $V_{TH}$ = 1.5 V, $I_{ON}/I_{OFF}$ = 1.1 × $10^8$) and stability ($V_{TH}$ shift of 1.5, −0.5 and −2.5 V for positive bias-stress, negative bias-stress, and thermal stress tests, respectively) than the a-IGZO:N/a-IZO:N TFTs. Based on the X-ray photoemission spectroscopy measurements and energy band analysis, we assumed that the optimized interface trap states, the less ambient gas adsorption, and the better suppression of oxygen vacancies in the a-IZO:N/a-IGZO:N hetero-structures might explain the better behavior of the corresponding TFTs.

**Keywords:** amorphous oxide semiconductor (AOS); thin film transistor (TFT); nitrogen-doped amorphous InGaZnO (a-IGZO:N); nitrogen-doped amorphous InZnO (a-IZO:N); hetero-structure

## 1. Introduction

Amorphous oxide semiconductors (AOS), including amorphous InGaZnO (a-IGZO), amorphous InZnO (a-IZO), amorphous InGaO (a-IGO), etc., have been widely investigated as the channel layers of thin-film transistors (TFTs) since 2004 [1]. In fact, AOS TFTs are one of the major candidates to replace silicon TFTs for driving active-matrix liquid crystal displays (AMLCDs) and active-matrix organic light-emitting diodes (AMOLEDs) because of their high field-effect mobility ($\mu_{FE}$~10 $cm^2 \cdot V^{-1} \cdot s^{-1}$), good uniformity (substrate size could reach 2200 × 2500 mm or even larger), simple processing methods, etc. [2–5]. However, further improvements over the performance and stability of AOS TFTs are still needed for practical applications in flat panel displays (FPDs) and the other fields.

Arai et al. [6] used amorphous InSnZnO (a-ITZO) as the channel layers of TFTs and designed low RC-delay device structures to optimize the performance and reliability of pixel and driving circuits for AMOLEDs. Hsu et al. [7] improved the stability of a-IGZO TFTs by using the asymmetric device structure. Lin et al. [8] co-sputtered IGZO and Al to form stable IGZAO TFTs [8]. Mativenga et al. [9] prepared the rollable a-IGZO TFTs with good bias stability, good mechanical stability, and high operation frequency (~400 kHz) by using the solution-processed colorless-polyimide as the substrates [9].

Recently, nitrogen-doping (N-doping) was shown to effectively improve the electrical properties (e.g., sub-threshold swing (SS), bias-stress stability, etc.) of AOS TFTs (e.g., a-IGZO:N TFTs [10], a-IZO:N TFTs [11], etc.). The N-doping decreased the channel/dielectric interface trap density, as well as the density of deep states, and the concentration of oxygen vacancies ($V_O$) in the channel layers of

a-IGZO TFTs [12]. Our previous work [13] indicated that N-doping improved the device performance and stability of a-IGZO TFTs by moderately adjusting the *Vo* concentration and largely suppressing the defects formation in the bulk channels, which was different from undoping and oxygen doping (O-doping). On the other side, N-doping unexpectedly degraded the mobility in a-IGZO:N [12], a-IZO:N [14], and ZnO:N [15], which might be attributed to the suppression of *Vo*, the main source of free electrons in AOS films [16].

Another effective improving method is to form double-stacked channel layers (DSCL) for AOS TFTs, which has been studied by our group [17,18], Chong et al. [19], and Jeon et al. [20]. Among these studies, the DSCL structure was shown to be valid at improving the electrical characteristics (e.g., $\mu_{FE}$, bias-stress stability, etc.) of TFTs. These improvements might result from the hetero-structure channel layers in DSCL devices [21–23]. In our recent reports, we obtained the DSCL structure by combining the a-IZO film with a-IGZO:N films, which made the corresponding TFTs exhibit quite a large $\mu_{FE}$ (49.6 $cm^2 \cdot V^{-1} \cdot s^{-1}$) but too negative threshold voltage ($V_{TH}$ ~−2.3 V) [24,25]. Therefore, further improvement is still necessary.

In this study, we used a-IZO:N rather than a-IZO to combine with a-IGZO:N and formed two novel DSCL structures (a-IGZO:N/a-IZO:N and a-IZO:N/a-IGZO:N), achieving a good electrical performance and good stability of the corresponding TFT devices.

## 2. Materials and Methods

The inverted staggered AOS TFTs were fabricated on the p++ silicon wafers with 100-nm-thick thermal oxide ($SiO_2$). The silicon wafers and thermal oxide films served as the gate electrodes and gate insulators, respectively. As shown in Figure 1, two types of N-doped DSCL TFTs were prepared for comparison, i.e., Samples I (a-IGZO:N/a-IZO:N) and II (a-IZO:N/a-IGZO:N).

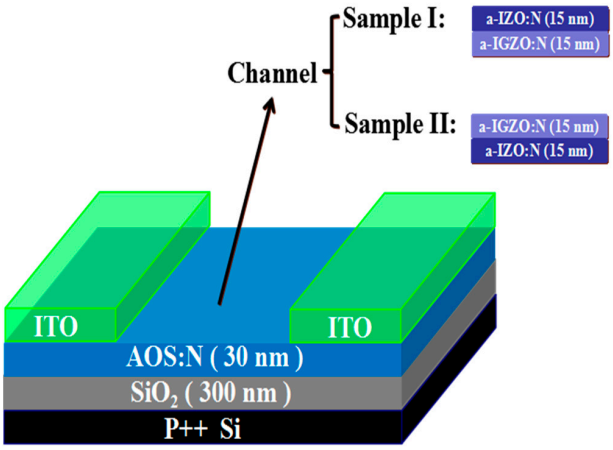


**Figure 1.** Schematic cross-section of the N-doped double-stacked channel layers (DSCL) thin film transistors (TFTs) (Samples I and II).

Here, the channel layers and source/drain (S/D) electrodes were all deposited by a sputtering machine (SYSKEY Automatic Muti-targets Sputtering System, Hsinchu, Taiwan). The chamber was evacuated to base-pressure (lower than $3 \times 10^{-6}$ Torr), and then the pressure was fixed at $3 \times 10^{-3}$ Torr during film deposition. The a-IGZO:N films were deposited by RF magnetron sputtering at room temperature (RT) using an a-IGZO target ($In_2O_3$:$Ga_2O_3$:ZnO = 1:1:1 mol % ) with a plasma power of 60 W and an Ar flow rate of 10 sccm (sccm denotes cubic centimeter per minute at STP); the nitrogen gas ($N_2$) was introduced in situ into the chamber at a flow rate of 1.2 sccm. The deposition of a-IZO:N films was performed by RF magnetron sputtering at RT using an a-IZO target ($In_2O_3$:ZnO = 3:1 mol %) with a plasma power of 70 W. The $N_2$ was fed in situ into the chamber at a flow rate of 2.5 sccm; the flow rates of Ar and $O_2$ gas were fixed at 20 and 7 sccm, respectively. After depositing the channel layers,

the 100-nm-thick indium-tin-oxide (ITO) layers were prepared as S/D electrodes by RF magnetron sputtering. During sputtering, the shadow masks were used to define the patterns of the channel layers and S/D electrodes. Finally, the samples were annealed at 573 K for 1 h in $N_2$ atmosphere.

In this study, the channel width ($W$) and length ($L$) of the tested TFTs were fixed as 1000 and 250 μm, respectively. The electrical measurements for all the devices were employed using an electrical analyzer (Keithley 4200, Keithley Instruments, Inc., Beaverton, OR, USA). An X-ray photoemission spectroscopy (XPS, ESCLAB 250Xi, Thermal-fisher, Waltham, MA, USA) was used to analyze the O1s peaks for the a-IGZO:N and a-IZO:N thin films. An atomic force microscopy (AFM, Bruker ICON, Tucson, AZ, USA) was used to characterize the surface properties of a-IGZO:N and a-IZO:N thin films.

## 3. Results

Figure 2 shows the O1s XPS spectra of a-IGZO:N and a-IZO:N thin films. The same processing conditions for the film depositions were used as were adopted for the corresponding TFTs. The spectra were calibrated by tacking the C1s (~284.8 eV) reference. Figure 2a,b show the de-convolution of O1s XPS spectra for the a-IGZO:N and a-IZO:N thin films, respectively. Gaussian fitting was used to de-convolve the O1s peaks, which could be fitted by three components, centered approximately at $530 \pm 0.1$ eV ($O_1$ peak), $531 \pm 0.3$ eV ($O_2$ peak), and $532 \pm 0.2$ eV ($O_3$ peak). The $O_1$ peak is supposed to reflect the oxide lattices in the stoichiometric wurtzite structure without oxygen deficiency; the $O_2$ peak represents the oxide lattices in the oxygen-deficient region ($V_O$). The $O_3$ peak is usually considered to be related to the chemisorbed hydroxide (e.g., moisture etc.) [26–28].

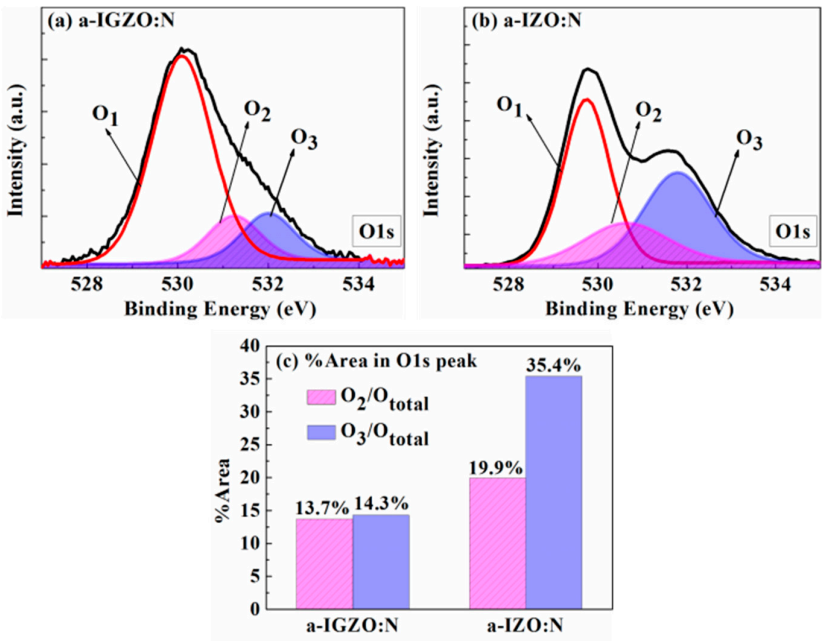


**Figure 2.** The X-ray photoemission spectroscopy (XPS) measurement and analysis results: (**a**) O1s spectra of the a-IGZO:N film; (**b**) O1s spectra of the a-IZO:N film; and (**c**) %Area of each component in O1s detected by XPS.

To quantitatively study each component of the O1s peak, we defined the Area and %Area to denote the de-convolution area and the de-convolution area percentage of each sub-peak over the O1s peak as follows:

$$\mathrm{Area}(O_{total}) = \mathrm{Area}(O_1) + \mathrm{Area}(O_2) + \mathrm{Area}(O_3), \quad (1)$$

$$\%\mathrm{Area}(O_2/O_{total}) = \mathrm{Area}(O_2)/\mathrm{Area}(O_{total}) \times 100\%, \quad (2)$$

$$\%\mathrm{Area}(O_3/O_{total}) = \mathrm{Area}(O_3)/\mathrm{Area}(O_{total}) \times 100\%. \quad (3)$$

As shown in Figure 2c, the %Area ($O_2/O_{total}$) and %Area ($O_3/O_{total}$) of a-IGZO:N films were 13.7% and 14.3%, respectively. However, the %Area ($O_2/O_{total}$) and %Area ($O_3/O_{total}$) of a-IZO:N films were much larger (19.9% and 35.4%), implying that there were more $V_O$ and trap states in the a-IZO:N films relative to those in the a-IGZO:N films. In addition, the a-IZO:N films tended to adsorb much more moisture gas at the film surface than the a-IGZO:N films.

Figure 3 shows the root mean square (RMS) roughness and resistivity of a-IGZO:N and a-IZO:N thin films. The roughness of a-IGZO:N film (0.28 nm) was a little larger than that of a-IZO:N film (0.21 nm). In addition, the a-IZO:N exhibited a much smaller resistivity (2.7 Ωcm) than the a-IGZO:N (58 Ωcm ). This might be because a-IZO:N contained more $V_O$ (electrons) than a-IGZO:N. This agreed well with the XPS measurement data (as shown in Figure 2).

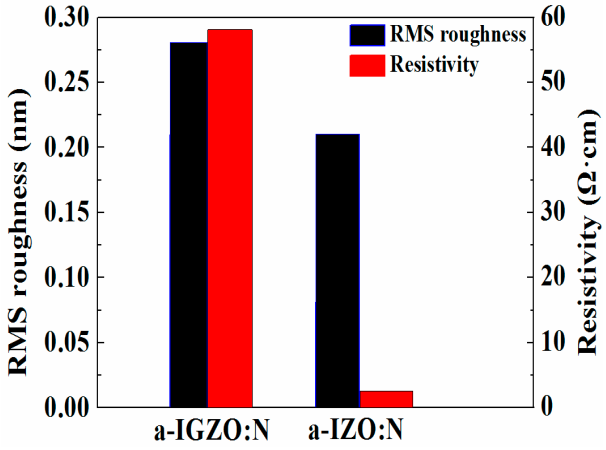


**Figure 3.** Root mean square (RMS) roughness and resistivity of a-IGZO:N and a-IZO:N thin films.

Figure 4 shows the transfer curves of the AOS TFTs with a-IGZO:N/a-IZO:N (Sample I) and a-IZO:N/a-IGZO:N (Sample II) channel layers, respectively. The corresponding performance parameters were extracted and listed in Table 1. Here, the $\mu_{FE}$ was calculated from the maximum slope, that was extracted graphically from the square root of drain current, $I_{DS}{}^{1/2}$, versus gate voltage, $V_{GS}$, in the saturation region [29,30]. The $V_{TH}$ was achieved from the gate voltage value where $I_{DS}/(W/L)$ = 100 nA. The SS was obtained from the half value of the difference between the gate voltages corresponding to the drain current of $10^{-10}$ A and $10^{-8}$ A, respectively. The on-off current ratio ($I_{ON}/I_{OFF}$) was defined as the ratio of the maximum turn-on current to the minimum turn-off current.

Conventional AOS TFTs, i.e., the devices with single channel-layers (a-IGZO TFTs, a-IGZO:N TFTs, etc.), generally have $\mu_{FE}$ of less than 10 $cm^2 \cdot V^{-1} \cdot s^{-1}$ [10,12,31]. The N-doped DSCL TFTs (Samples I and II), however, exhibited apparent improvements in their field-effect mobilities, as shown in Table 1. If we compare these two samples, Sample II showed even better electrical performance on the whole than Sample I, although its field-effect mobility (15.0 $cm^2 \cdot V^{-1} \cdot s^{-1}$) was smaller than that of Sample I (31.9 $cm^2 \cdot V^{-1} \cdot s^{-1}$). To be specific, Sample II exhibited a more positive $V_{TH}$ (1.5 V) and a smaller SS value (0.5 V/dec) than Sample I. As shown in Table 1, $I_{ON}/I_{OFF}$ values of both the samples were larger than $10^8$.

**Table 1.** Extracted performance parameters of the N-doped DSCL TFTs.

| Sample | $\mu_{FE}$ ($cm^2 \cdot V^{-1} \cdot s^{-1}$) | SS (V/dec) | $V_{TH}$ (V) | $I_{ON}/I_{OFF}$ |
|---|---|---|---|---|
| I | 31.9 | 0.8 | −5.0 | $1.2 \times 10^8$ |
| II | 15 | 0.5 | 1.5 | $1.1 \times 10^8$ |

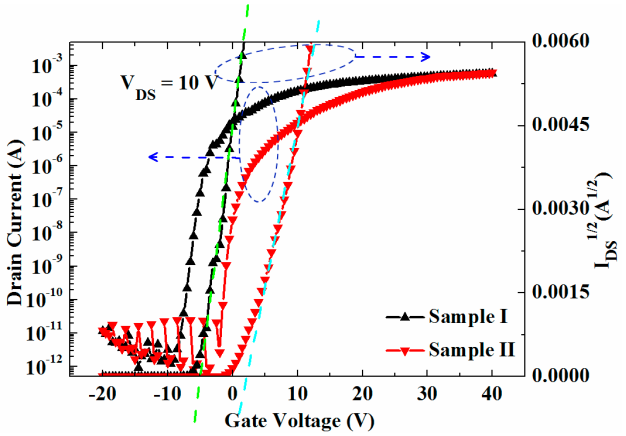


**Figure 4.** Transfer curves of the N-doped DSCL TFTs (Samples I (a-IGZO:N/a-IZO:N TFT) and II (a-IZO:N/a-IGZO:N TFT)).

Figure 5 shows the transfer curves evolution of the N-doped DSCL TFTs under positive bias stress (PBS) and negative bias stress (NBS) tests for 2500 s, respectively. Here, the gate electrodes were stressed at +30 V for PBS and −30 V for NBS for a period and then the transfer curves were instantly measured. As shown in Figure 5a,b, Sample I showed more stable PBS properties with a smaller $V_{TH}$ shift of +0.5 V, whereas Sample II exhibited a little larger $V_{TH}$ shift (+1.5 V) for the PBS duration. However, during NBS testing (Figure 5c,d), the $V_{TH}$ shift of Sample I became much worse (−9.0 V) than that of Sample II (−0.5 V). In short, Sample I showed better PBS stability ($V_{TH}$ shift of +0.5 V) and Sample II exhibited much more stableelectrical properties ($V_{TH}$ shift of −0.5 V) for NBS tests.

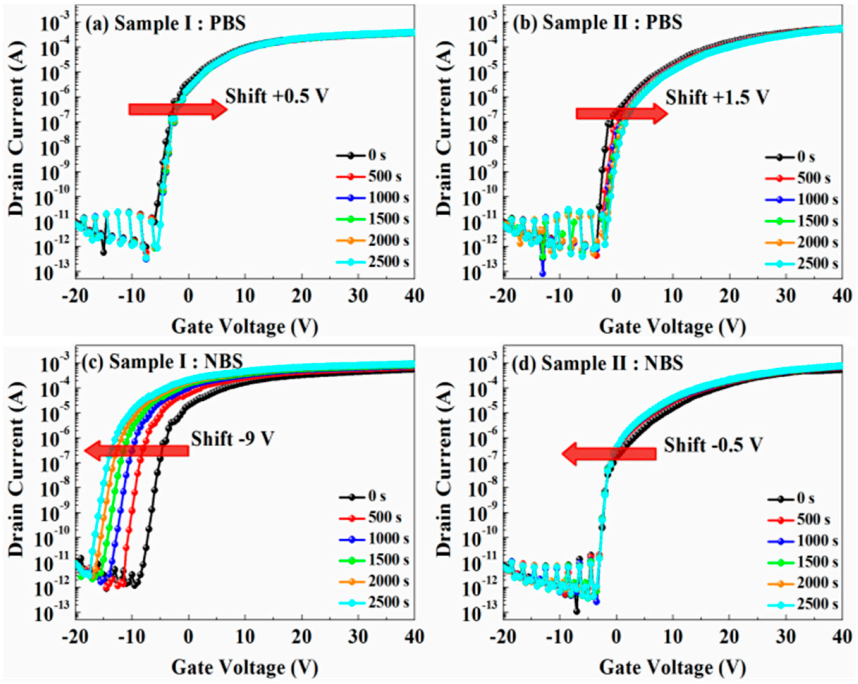


**Figure 5.** Bias stress stability of the N-doped DSCL TFTs: (**a**) positive bias stress (PBS) of the a-IGZO:N/a-IZO:N TFT (Sample I); (**b**) PBS of the a-IZO:N/a-IGZO:N TFT (Sample II); (**c**) negative bias stress (NBS) of the a-IGZO:N/a-IZO:N TFT (Sample I); and (**d**) NBS of the a-IZO:N/a-IGZO:N TFT (Sample II). The stressing conditions were $V_{GS}$ = +30 for PBS and $V_{GS}$ = −30 for NBS. The transfer curves were obtained with $V_{DS}$ = 10 V.

Figure 6 shows the transfer curve evolution of the N-doped DSCL TFTs under thermal stress. From here, one might notice that these two samples exhibited markedly different negative $V_{TH}$ shifts. As shown in Figure 6, the $V_{TH}$ of Sample I shifted up to −11.5 V as the temperature increased from 298 to 398 K, indicating that Sample I had muchworsethermal stability. In comparison, Sample II was more stable under thermal stress, with a $V_{TH}$ that only shifted −2.5 V.

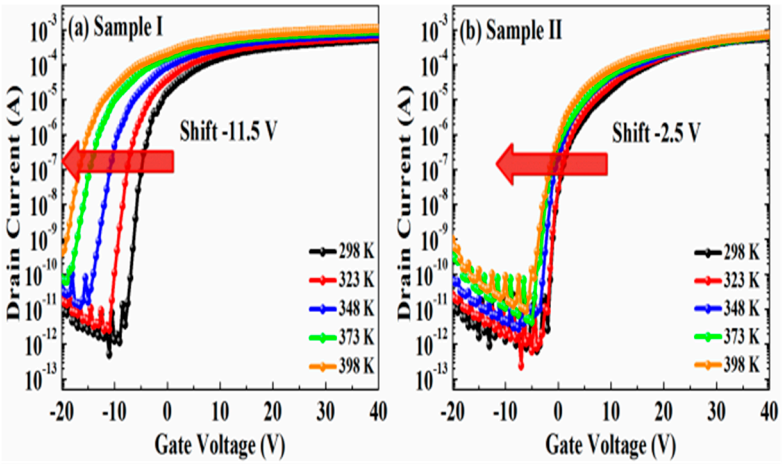


**Figure 6.** Thermal stress of the N-doped DSCL TFTs: (**a**) a-IGZO:N/a-IZO:N TFT (Sample I); (**b**) a-IZO:N/a-IGZO:N TFT (Sample II). The transfer curves were obtained with $V_{DS}$ = 10 V.

Here we summarize the interesting results related to the N-doped DSCL TFTs. The $\mu_{FE}$ of AOS TFTs could be largely improved by using the DSCL composed of a high-defect-density channel layer and a low-defect-density channel layer to form the hetero-junction structure [19,21]. In this study, we deliberately designed and prepared the N-doped DSCL TFTs (Samples I and II) using the hetero-structure channel layers composed of a 15-nm-thick a-IZO:N layer and a 15-nm-thick a-IGZO:N layer, and finally obtained good electrical performance (e.g., the large $\mu_{FE}$, the proper $V_{TH}$, the small SS, and the large $I_{ON}/I_{OFF}$), as shown in Table 1. On the other hand, although Sample I exhibited a larger field-effect mobility ($\mu_{FE}$ = 31.9 $cm^2 \cdot V^{-1} \cdot s^{-1}$), its $V_{TH}$ was rather negative (−5.0 V), which was apparently not fit for driving FPDs. Sample II showed the optimum device performance ($\mu_{FE}$ = 15.0 $cm^2 \cdot V^{-1} \cdot s^{-1}$, $V_{TH}$ = 1.5 V, SS = 0.5 V/dec) relative to Sample I. In addition, Sample I exhibited excellent PBS stability ($V_{TH}$shift = +0.5 V), whereas its NBS ($V_{TH}$ shift = −9.0 V) and thermal stability ($V_{TH}$ shift = −11.5 V) were poor. Compared to Sample I, more stable properties were observed for Sample II during NBS ($V_{TH}$ shift = −0.5 V) and thermal stress ($V_{TH}$ shift = −2.5 V) tests. Therefore, Sample II, rather than Sample I, was preferred because of its better electrical performance and stability. However, what accounted for these results? The related physical mechanisms should be ascertained by analyzing the microstructures and energy bands of the channel layers for these TFT devices.

Figure 7 shows energy band diagrams of the two samples when $V_{GS} >> V_{TH}$. As mentioned in the literature [15], $V_O$ was considered as the main source of free electrons in AOS films. According to the XPS result and the film resistivity (Figures 2 and 3), the a-IZO:N film contained more $V_O$ and exhibited a smaller resistivity with respect to the a-IGZO:N film, indicating that there could be even more electrons in the a-IZO:N film than those in the a-IGZO:N film. Due to the differences in carrier concentrations, the electrons injected from the a-IZO:N layer into the a-IGZO:N layer and formed the built-in electrical voltage ($V_{built\text{-}in}$) near the interfacial region between the a-IZO:N and a-IGZO:N films. The $V_{built\text{-}in}$ might cause injection electrons to accumulate in the interface region between the a-IZO:N and a-IGZO:N layers. In addition, the polarity of $V_{built\text{-}in}$ was opposite for Samples I and II, as shown in Figure 7.

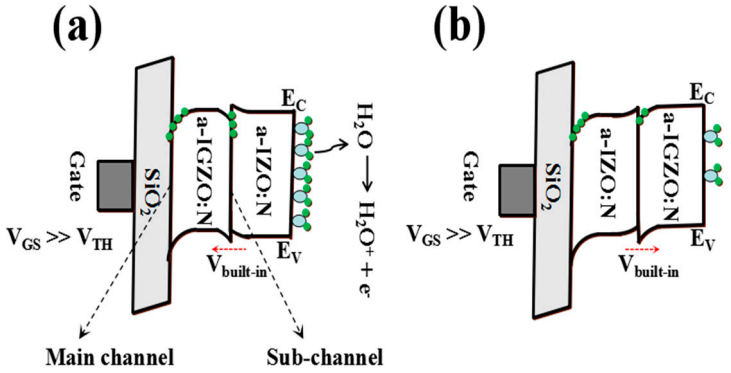


**Figure 7.** The energy band diagrams for (**a**) a-IGZO:N/a-IZO:N TFT (Sample I) and (**b**) a-IZO:N/a-IGZO:N TFT (Sample II), when $V_{GS}$>>$V_{TH}$.

The N-doped DSCL AOS TFTs (Samples I and II) exhibited large $\mu_{FE}$, which resulted from the presence of double channels due to the hetero-structure channel layers in these samples. As shown in Figure 7a,b, some electrons might accumulate at the interfacial region between the a-IGZO:N layer and a-IZO:N layer due to the difference of the carrier concentration, as well as the formation of $V_{built\text{-}in}$. Apparently, these accumulated electrons could also participate in current conduction, forming a sub-channel at the a-IGZO:N/a-IZO:N or a-IZO:N/a-IGZO:N interfacial regions during the operation of the TFT devices. In other words, the current conduction operation of the DSCL AOS TFTs was dominated by not only the main-channel (the interface between channel layer and gate insulator), but also the sub-channel (the interface between a-IGZO:N and a-IZO:N films). The co-contribution of these two channels in current conduction led to the large $\mu_{FE}$ in the hetero-structure AOS TFTs.

In particular, among the DSCL devices, Sample I exhibited larger $\mu_{FE}$ (31.9 $cm^2 \cdot V^{-1} \cdot s^{-1}$) than Sample II (15.0 $cm^2 \cdot V^{-1} \cdot s^{-1}$), which could be explained by the hetero structures in their energy bands when $V_{GS}$>>$V_{TH}$. As shown in Figure 7a,b, moisture gas molecules could diffuse in and out of AOS thin films, donating extra electrons. This might largely influence the device performance ($\mu_{FE}$, SS, $V_{TH}$, etc.) [32]. As mentioned before, from the XPS measurements, the a-IZO:N film adsorbed much more ambient moisture gas than the a-IGZO:N films. Thus, there could be many more extra electron donations caused by moisture gas adsorption in Sample I than those in Sample II. This implied that many more extra electrons accumulated at the sub-channel in Sample I, participating in the current conduction when $V_{GS}$>>$V_{TH}$, and thus leading to a larger $\mu_{FE}$ and a more negative $V_{TH}$ in Sample I relative to those in Sample II. According to Reference [32], moisture adsorption could bring about SS deterioration in AOS TFTs. Hence, as shown in Table 1, Sample I exhibited a worse SS value (0.8 V/dec) than Sample II, possibly due to the more moisture adsorptions in its channel layer.

For the applications of TFTs in AMLCDs and AMOLEDs, it is important to keep $V_{TH}$ of 0 V (or a little larger). In our previous study [25], we designed a-IZO/a-IGZO:N TFTs, whose $\mu_{FE}$ was quite large (49.6 $cm^2 \cdot V^{-1} \cdot s^{-1}$), but $V_{TH}$ was too negative (−2.3 V). In this study, however, Sample II (a-IZO:N/a-IGZO:N TFT) had a positive $V_{TH}$ of 1.5 V, which might result from the fact that N-doping decreased the trap states in a-IZO and at the front channel interface [12,13].

As shown in Figure 5a,b, the N-doped DSCL TFTs (Samples I and II) showed different PBS stability. Sample I had better PBS stability than Sample II. The stability of AOS TFTs could be influenced by the ambient $O_2$ gas during the PBS testing [10,25,32]. The reaction might be described as:

$$O_{2(gas)} + e^- \rightarrow {O_{2(solid)}}^-. \quad (4)$$

The better PBS stability of Sample I could be attributed to the more moisture gas adsorptions on the film surface, which weakened the $O_2$ adsorption to the channel.

NBS tests might cause a moisture reaction at the back channels of AOS TFTs, which could be described as [25,32,33]:

$$H_2O^- \rightarrow H_2O + e^-. \quad (5)$$

The XPS results indicated that the a-IZO:N films more easily adsorbed the ambient moisture gas than the a-IGZO:N films (Figure 2). Figure 5c,d indicate that Sample I showed very poor NBS stability ($V_{TH}$ shift = −9 V). This was likely because the sub-channel of Sample I (a-IGZO:N/a-IZO:N interface) was greatly influenced by the ambient moisture gas during the NBS testing. In contrast, Sample II showed a much smaller $V_{TH}$ shift (−0.5 V) under NBS tests. This might be due to the weak moisture adsorption effect of the a-IGZO:N layer, which was consistent with the XPS data (Figure 2).

Thermal stability data in Figure 6 indicated that Sample I was unstable ($V_{TH}$ shift = −11.5 V) under thermal stressing; Sample II was much more thermally stable ($V_{TH}$ shift = −2.5 V). We reported that larger concentration variation of $V_O$ in AOS TFTs could lead to serious $V_{TH}$ shift during the thermal testing [29]. In addition, the literature [16,34] indicated that N-doping suppressed $V_O$ formation in the bulk channels for the thermal tests of a-IGZO:N TFTs. Hence, the better thermal stability of Sample II might be attributed to the a-IGZO:N films, which acted as a passivation layer and suppressed the $V_O$ formation in the a-IZO:N layers.

## 4. Conclusions

We prepared and characterized the N-doped TFTs with the hetero-structure channel layers composed of 15-nm-thick a-IZO:N and 15-nm-thick a-IGZO:N. Two DSCL structures (a-IGZO:N/a-IZO:N and a-IZO:N/a-IGZO:N) were designed and studied to serve as the channel layers of AOS TFTs. Generally, the N-doped DSCL TFTs exhibited a large field-effect mobility (up to 31.9 $cm^2 \cdot V^{-1} \cdot s^{-1}$) due to the presence of double conduction channels during electrical operations. As compared with the a-IGZO:N/a-IZO:N TFT, the a-IZO:N/a-IGZO:N TFT showed better electrical performance ($\mu_{FE}$ = 15.0 $cm^2 \cdot V^{-1} \cdot s^{-1}$, SS = 0.5 V/dec, $V_{TH}$ = 1.5 V, $I_{ON}/I_{OFF} = 1.1 \times 10^8$) and more stable properties ($V_{TH}$ shift of +1.5, −0.5 and −2.5 V, for PBS, NBS, and thermal tests, respectively). These results were likely due to the optimized hetero structure, the less ambient moisture adsorption, and the better suppression effect of the $V_O$ formation.

**Acknowledgments:** This work was supported by National Natural Science Foundation of China (Grant No. 61474075). Haiting Xie thanks for the support from Department of Photonics and Display Institute, National Chiao Tung University.

**Author Contributions:** Haiting Xie fabricated and measured all the TFT devices. Haiting Xie and Chengyuan Dong designed the experiments and contributed to the theoretical explanations. The manuscript was written by Haiting Xie and Chengyuan Dong, and was revised by all the authors.

**Conflicts of Interest:** The authors declare no conflict of interest.

## References

1. Nomura, K.; Ohta, H.; Takagi, A.; Kamiya, T.; Hirano, M.; Hosono, H. Room-temperature fabrication of transparent flexible thin-film transistors using amorphous oxide semiconductors. *Nature* **2004**, *432*, 488–492. [CrossRef] [PubMed]
2. Nomura, K.; Kamiya, T.; Ikenaga, E.; Yanagi, H.; Kobayashi, K.; Hosono, H. Depth analysis of sub-gap electronic states in amorphous oxide semiconductor, a-In-Ga-Zn-O, studied by hard X-ray photoelectron spectroscopy. *J. Appl. Phys.* **2013**, *109*, 073726. [CrossRef]
3. Lee, J.S.; Chang, S.; Koo, S.M.; Lee, S.Y. High-performance a-IGZO TFT with $ZrO_2$ gate dielectric fabricated at room temperature. *IEEE Electron Device Lett.* **2010**, *31*, 225–227. [CrossRef]
4. Wang, Y.L.; Ren, F.; Lim, W.; Norton, D.P.; Pearton, S.J.; Kravchenko, I.I.; Zavada, J.M. Room temperature deposited indium zinc oxide thin film transistors. *Appl. Phys. Lett.* **2011**, *90*, 232103. [CrossRef]
5. Fortunato, E.; Barquinha, P.; Goncalves, G.; Pereira, L.; Martins, R. High mobility and low threshold voltage transparent thin film transistors based on amorphous indium zinc oxide semiconductors. *Solid State Electron.* **2008**, *90*, 443–448. [CrossRef]

6. Arai, T.; Sasaoka, T. Emergent oxide TFT technologies for next-generation AM-OLED displays. *SID Symp. Dig. Tech. Papers* **2011**, *42*, 710–713. [CrossRef]
7. Hsu, C.C.; Wu, C.H.; Ting, W.C. Stability improvement of amorphous InGaZnO TFTs by an asymmetric design. *Electron. Lett.* **2015**, *51*, 1534–1536. [CrossRef]
8. Lin, Y.H.; Lee, C.T. Stability of Indium Gallium Zinc Aluminum oxide thin-film transistors with treatment processes. *J. Electron. Mater.* **2017**, *46*, 1–5. [CrossRef]
9. Mativenga, M.; Li, X.; Um, J.; Geng, D.; Jin, S.; Jang, J. Highly-stable and transparent oxide TFTs for rollable displays. *Symp. Dig. Tech. Papers* **2015**, *46*, 883–886. [CrossRef]
10. Liu, P.T.; Chou, Y.T.; Teng, L.F.; Li, F.H.; Shieh, H.P. Nitrogenated amorphous InGaZnO thin film transistor. *Appl. Phys. Lett.* **2011**, *98*, 052102. [CrossRef]
11. Han, Y.; Yan, H.; Tsai, Y.C.; Li, Y.; Zhang, Q.; Shieh, H.P.D. Influences of nitrogen doping on the electrical characteristics of Indium-Zinc-Oxide thin film transistors. *IEEE Trans. Dev. Mater. Reliab.* **2016**, *16*, 642–646. [CrossRef]
12. Raja, J.; Jang, K.; Balaji, N.; Choi, W.; Trinh, T.T.; Yi, J. Negative gate-bias temperature stability of N-doped InGaZnO active-layer thin-film transistors. *Appl. Phys. Lett.* **2013**, *102*, 083505. [CrossRef]
13. Xie, H.; Xu, J.; Liu, G.; Zhang, L.; Dong, C. Development and analysis of nitrogen-doped amorphous InGaZnO thin film transistors. *Mater. Sci. Semicond. Process.* **2017**, *64*, 1–5. [CrossRef]
14. Ortega, J.J.; Aguilar-Frutis, M.A.; Alarcón, G.; Falcony, C.; Méndez-Garcíab, V.H.; Araiza, J.J. Band gap engineering of indium zinc oxide by nitrogen incorporation. *Mater. Sci. Eng. B* **2014**, *187*, 83–88. [CrossRef]
15. Lim, A.S.J.; Kwon, S.J.; Kim, H.; Park, J.S. High performance thin film transistor with low temperature atomic layer deposition nitrogen-doped ZnO. *Appl. Phys. Lett.* **2007**, *91*, 183513. [CrossRef]
16. Ryu, B.; Noh, H.K.; Choi, E.A.; Chang, K.J. O-vacancy as the origin of negative bias illumination stress instability in amorphous In–Ga–Zn–O thin film transistors. *Appl. Phys. Lett.* **2010**, *97*, 022108. [CrossRef]
17. Zhan, R.; Dong, C.; Yang, B.R.; Shieh, H.P.D. Modulation of interface and bulk states in amorphous InGaZnO thin-film transistors with double stacked channel layers. *J. Appl. Phys.* **2013**, *52*, 090205. [CrossRef]
18. Zhan, R.; Dong, C.; Liu, P.T.; Shieh, H.P.D. Influence of channel layer and passivation layer on the stability of amorphous InGaZnO thin film transistors. *Microelectron. Reliab.* **2013**, *53*, 1879–1885. [CrossRef]
19. Chong, E.; Lee, S.Y. Influence of a highly doped buried layer for HfInZnO thin-film transistors. *Semicond. Sci. Technol.* **2011**, *27*, 012001. [CrossRef]
20. Jeon, S.; Ahn, S.E.; Song, I.; Jeon, Y.; Kim, Y.; Kim, S.; Choi, H.; Kim, H.; Lee, E.; Lee, S.; et al. Dual gate photo-thin film transistor with high photoconductive gain for high reliability, and low noise flat panel transparent imager. In Proceedings of the IEEE International Electron Devices Meeting (IEDM), Washington, DC, USA, 5–7 December 2017. [CrossRef]
21. Park, J.C.; Lee, H.N. Improvement of the performance and stability of oxide semiconductor thin-film transistors using double-stacked active layers. *IEEE Electron Dev. Lett.* **2012**, *33*, 818–820. [CrossRef]
22. Lee, S.; Nathan, A.; Robertson, J. Challenges in visible wavelength detection using optically transparent oxide semiconductors. *IEEE Sens.* **2012**, 1–4. [CrossRef]
23. Lee, S.; Jeon, S.; Robertson, J.; Nathan, A. How to achieve ultra high photoconductive gain for transparent oxide semiconductor image sensors. In Proceedings of the 2012 IEEE International Electron Devices Meeting (IEDM), San Francisco, CA, USA, 10–13 December 2012. [CrossRef]
24. Xie, H.; Wu, Q.; Xu, L.; Xu, J.; Zhang, L.; Liu, G.; Dong, C. Amorphous oxide thin film transistors with nitrogen-doped active layers. *SID Symp. Dig. Tech. Papers* **2016**, *47*, 1033–1036. [CrossRef]
25. Xie, H.; Wu, Q.; Xu, L.; Zhang, L.; Liu, G.; Dong, C. Nitrogen-doped amorphous oxide semiconductor thin film transistors with double-stacked channel layers. *Appl. Surf. Sci.* **2016**, *387*, 237–243. [CrossRef]
26. Jeong, B.; Ha, Y.G.; Moon, J.; Facchetti, A.; Marks, T.J. Role of gallium doping in dramatically lowering amorphous-oxide processing temperatures for solution-derived indium zinc oxide thin-film transistors. *Adv. Mater.* **2009**, *22*, 1346–1350. [CrossRef] [PubMed]
27. Yao, H.B.; Li, Y.; Wee, A.T.S. An XPS investigation of the oxidation/corrosion of melt-spun Mg. *Appl. Surf. Sci.* **2000**, *158*, 112–119. [CrossRef]
28. Frangini, S.; Giorgi, R.; Lascovich, J.; Mignone, A. XPS study of passive films formed ion an iron-aluminium intermetallic compound in acid solution. *Surf. Interface Anal.* **1994**, *21*, 435–441. [CrossRef]

29. Hu, Z.; Dong, C.; Zhou, D.; Chen, Y.; Wu, J.; Xie, H.; Chiang, C.L.; Chen, P.L.; Lai, T.C.; Lo, C.C.; et al. Thermal stability of amorphous InGaZnO thin-film transistors with different oxygen-contained active layers. *IEEE J. Disp. Technol.* **2015**, *11*, 610–614. [CrossRef]
30. Yaglioglu, B.; Yeom, H.Y.; Beresford, R.; Paine, D.C. High-mobility amorphous $In_2O_3$–10 wt % ZnO thin film transistors. *Appl. Phys. Lett.* **2006**, *89*, 062103. [CrossRef]
31. Sato, A.; Abe, K.; Hayashi, R.; Kumomi, H.; Nomura, K.; Kamiya, T.; Hirano, M.; Hosono, H. Amorphous In–Ga–Zn–O coplanar homojunction thin-film transistor. *Appl. Phys. Lett.* **2009**, *94*, 133502. [CrossRef]
32. Park, J.S.; Jeong, J.K.; Chung, H.J.; Mo, Y.G.; Kim, H.D. Electronic transport properties of amorphous indium-gallium-zinc oxide semiconductor upon exposure to water. *Appl. Phys. Lett.* **2008**, *92*, 072104. [CrossRef]
33. Liu, P.T.; Chou, Y.T.; Teng, L.F. Environment-dependent metastability of passivation-free indium zinc oxide thin film transistor after gate bias stress. *Appl. Phys. Lett.* **2009**, *95*, 233504. [CrossRef]
34. Raja, J.; Jang, K.; Balaji, N.; Yi, J. Suppression of temperature instability in InGaZnO thin-film transistors by in situ nitrogen doping. *Semicond. Sci. Technol.* **2013**, *28*, 115010. [CrossRef]